

# Entanglements and Crystallization of Concentrated Polymer Solutions: Molecular Dynamics Simulations

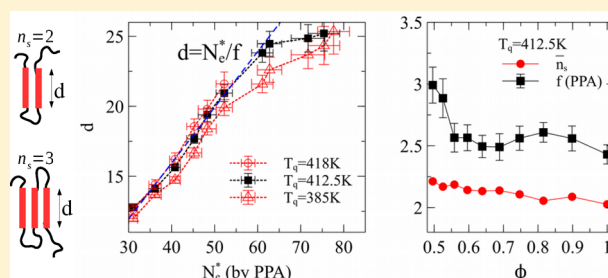
Chuanfu Luo,<sup>\*,†,‡,§</sup> Martin Kröger,<sup>§</sup> and Jens-Uwe Sommer<sup>†</sup>

<sup>†</sup>Leibniz-Institut für Polymerforschung Dresden e.V., Hohe Strasse 6, 01069 Dresden, Germany

<sup>‡</sup>Max Planck Institute of Colloids and Interfaces, Am Mühlenberg 1, 14476 Potsdam, Germany

<sup>§</sup>Polymer Physics, Department of Materials, ETH Zurich, CH-8093 Zurich, Switzerland

**ABSTRACT:** We carried out molecular dynamics simulations to study the crystallization of long polymers in a concentrated solution made by an explicit solvent of short chains. The weight-averaged entanglement length in the concentrated solution is found to exhibit power-law behavior with respect to the polymer volume fraction. The crystalline stem length obtained by quenching the solutions below melting temperature displays a linear relation with the entanglement length in the homogeneous solution above the crystallization temperature. Chain folding numbers are found to be very close to those in pure melts at different initial temperatures, and they tend to moderately decrease with increasing concentration of the long polymers. While our results are directly obtained from a coarse-grained model, they seem to suggest that the topological restriction of entanglements is a universal property to control the thickness selection during polymer crystallization.



## INTRODUCTION

More than 60% of industrial plastics are in the semicrystalline state, and the functional properties of these materials are directly related to their crystalline morphology.<sup>1,2</sup> The building blocks of crystalline morphologies are nanometer thin lamellae formed by more or less regularly folded chains which themselves can participate in several lamellae. Even at high supercooling, amorphous parts coexist with crystalline lamellae. This so-called semicrystalline state is important for the toughness and flexibility of polymer materials. Polymer crystallization processes take place under nonequibrated conditions accompanied by transitions between metastable states.<sup>3</sup> The complete understanding of polymer crystallization is a still unsolved problem.<sup>2,4,5</sup> One of the fundamental questions concerning polymer crystallization is what controls the lamellar thickness. The classical Lauritzen–Hoffman (LH) theory<sup>6–8</sup> based on concepts of secondary nucleation was challenged with respect to recent experiments on early stages of polymer crystallization.<sup>9</sup> Several alternative models have been proposed to capture different aspects of the polymer crystallization.<sup>9–13</sup> Computer simulations such as Monte Carlo (MC) and molecular dynamics (MD) have also provided insights into a further understanding of this process and to the issue of lamellar thickness.<sup>10,14–39</sup>

Upon adding solvents, the crystallization behavior of polymer chains can be changed, and the morphology of crystalline state can be affected drastically. For example, polymer single crystals can be obtained by slow growth from dilute solutions<sup>1</sup> as compared to the semicrystalline state one finds in melts. Generally, polymers crystallize slower from solutions with enhanced crystalline properties reflected by larger lamellar

thickness. This effect is usually interpreted by a growth rate that is sensitive to the degree of undercooling and thus slower in solution.<sup>1,4,5,8,11</sup> As shown in some experimental studies<sup>40–44</sup> and in our recent works,<sup>45–47</sup> entanglements in the melt state play an essential role for the selection of morphology and crystal thickness. This is in contrast to solutions, where polymer chains are sparsely distributed and the effective interactions between chains are weak. The degree of entanglement of polymer chains in a dilute solution is very low, and the topological restriction of entanglements to the crystallization might be considered as a minor effect. For the intermediate case of concentrated solutions, polymer chains are still highly entangled, and the effect of entanglements cannot be ignored. Even for crystallization from dilute solutions, the concentration of polymer chains is enhanced in the surface regions close to the preformed crystals, and the entanglement effect should also be considered. It is therefore interesting to study the effect of entanglements on the crystallization in concentrated solutions under variation of the polymer volume fraction. Using a polymer-like solvent, dilution allows us to vary the entanglement density without changing other parameters of the polymer system.

We begin by introducing the model and its implementation details, which includes a description and test of the equilibration protocol. Next, we present simulation results of concentrated polymer solutions. We calculate the entanglement lengths at different polymer volume fractions and discuss the

**Received:** September 29, 2016

**Revised:** November 23, 2016

**Published:** December 2, 2016

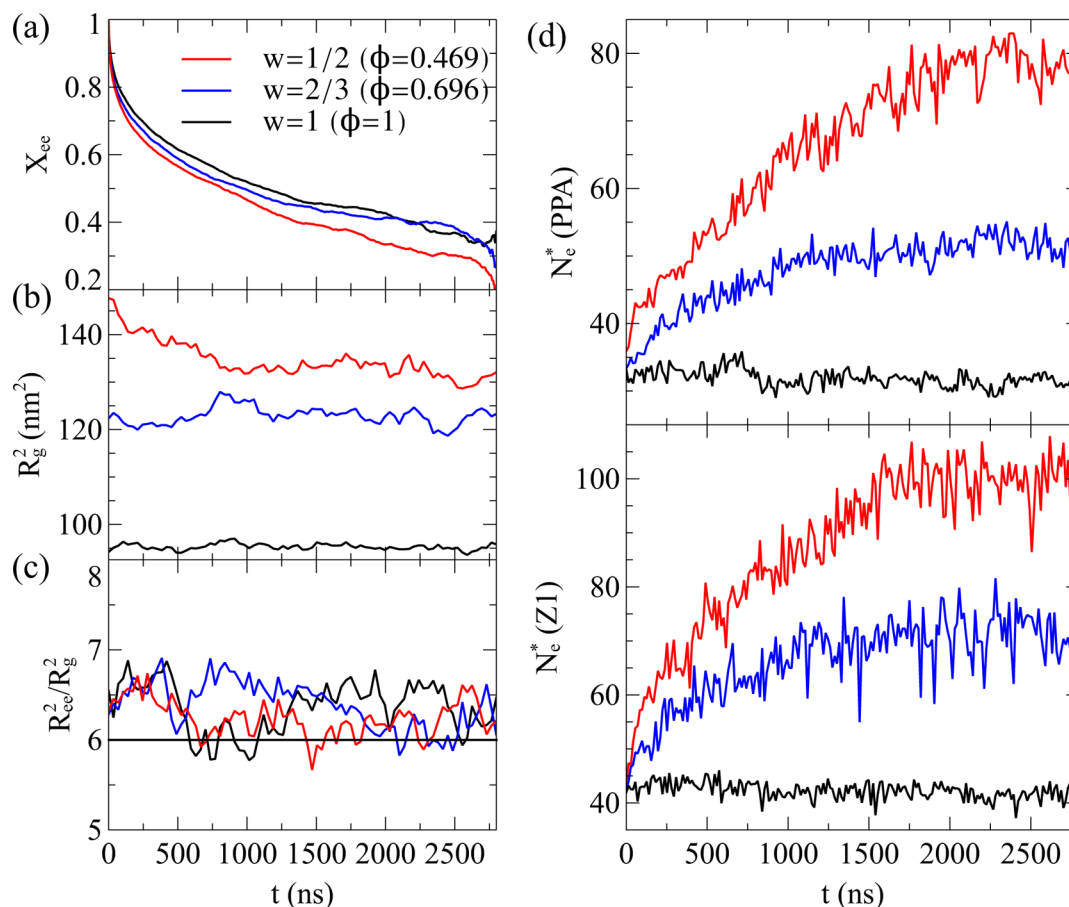


**Figure 1.** Conformational properties of the long polymer chains during equilibration for different polymer weight fractions ( $w$ ). (a) Autocorrelation function  $X_{ee}(t)$  of end-to-end vectors for the long chains. (b) Mean-square gyration radius  $\langle R_g^2(t) \rangle$ . (c) Ratio of mean-square end-to-end distance  $\langle R_{ee}^2(t) \rangle$  over the mean-square gyration radius. (d) Weight-averaged entanglement length  $N_c^*(t)$  calculated by PPA and Z1 methods. Different weight fractions  $w$  are marked by identical colors in all panels, as described in the legend of (a).

entanglement-related crystallization process. We are going to provide another evidence for a simple and universal concept to understand polymer crystallization that involves the topological restriction of entanglements.

## MODEL AND SIMULATION DETAILS

The simulation of polymer crystallization requires considering a coarse-grained representation of the components. The computational cost is otherwise prohibitive, as the crystallization process is slow, particularly in the presence of an explicit solvent. As shown in previous works by two of us,<sup>45,46,48–50</sup> the coarse-grained poly(vinyl alcohol) (CG-PVA) model proposed by Meyer and Müller-Plathe<sup>24</sup> is very suitable to study polymer crystallization. For the details of the model we refer the reader to previous works.<sup>24,48,50</sup> Reduced units are used in simulations, but we report the results with real units in the following discussions. For the CG-PVA model, the reduced length unit corresponds to the effective diameter (0.52 nm) of one PVA monomer, and the bond length is  $b_0 = 0.5$  (0.26 nm). The monomer mass  $m$  and Boltzmann constant  $k_B$  are both unity in reduced units. The reduced temperature  $T = 1$  corresponds to 550 K. Because of the simplification of coarse-graining, the dynamics in coarse-grained models is accelerated, particularly for short chains.<sup>51</sup> It was found previously that the reduced time unit corresponds to  $\approx 3.5$  ps by comparing the effective Rouse time of  $N = 20$ . The accelerated dynamics of

short chains may slightly affect the crystallization rate but not the entanglement length or lamellar thickness.

All MD simulations were carried out using the LAMMPS<sup>52</sup> package with our patch code for the CG-PVA model. The Verlet algorithm is used with a time step of 0.01 ( $\approx 35$  fs) to integrate Newton's equations of particle motions. The temperature is controlled by a Nosé–Hoover thermostat with a damp time of 100 MD steps ( $\approx 3.5$  ps). The pressure is controlled at 1 atm by a Berendsen barostat with a damp time of 1000 MD steps. The studied polymer system consists of 100 long chains with a polymerization degree  $N = 1000$ . Short chains with  $N = 5$  monomers per chain are used to model the explicit solvent. Both types of polymers are made of identical monomers. For concentrated conditions, different volume fractions of long chains are studied.

A primitive path analysis (PPA), following Everaers et al.,<sup>53</sup> and its geometric analogue, the Z1 method,<sup>54</sup> are used to calculate the primitive path network and the entanglement states of our simulated systems. Both PPA and Z1 methods operate on snapshots extracted from the MD trajectories and return lengths of the primitive path, and also entanglement kinks for the case of Z1, via annealing or geometric minimization of the sum of primitive path lengths. A primitive path shares its chain ends with the polymer, and primitive paths cannot cross each other. As the conformations of polymer chains are no longer Gaussian in melts near crystallization temperature,<sup>45</sup> we use the directly measured number of

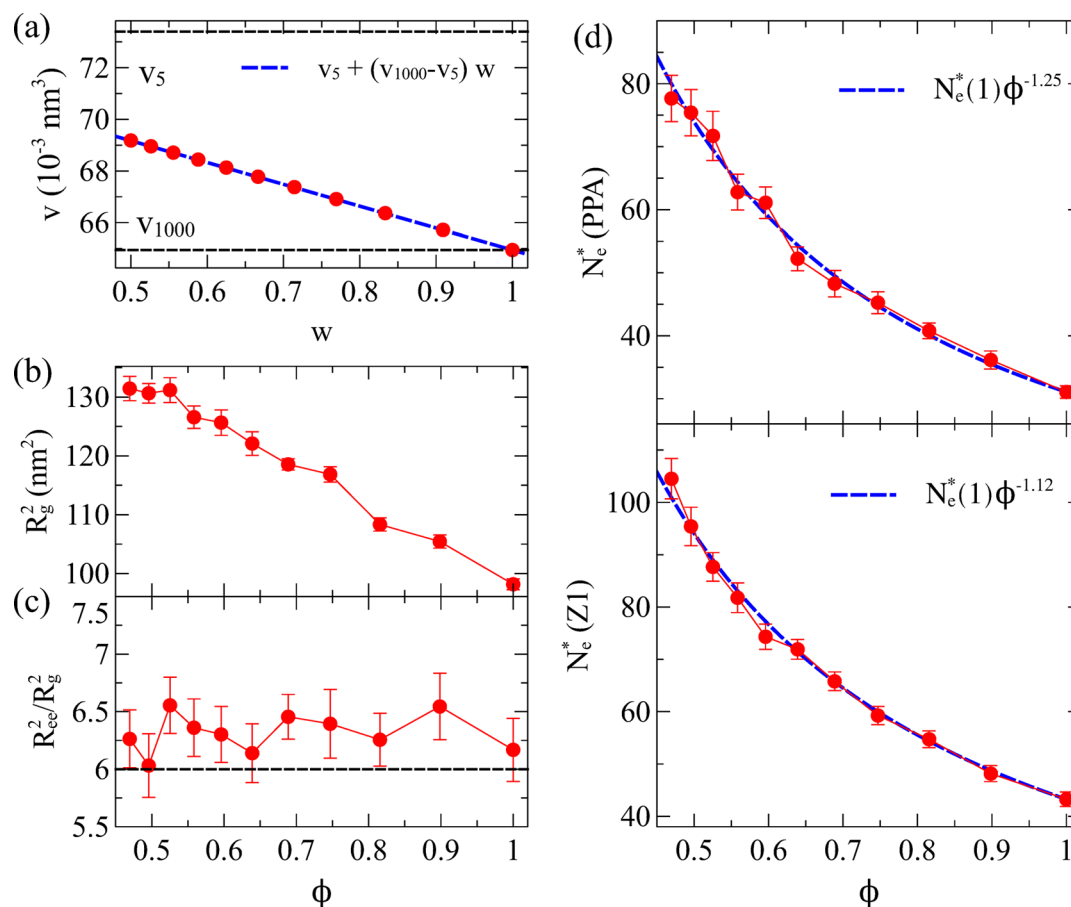


**Figure 2.** Equilibrium chain properties at different weight fractions  $w$  at  $T = 495$  K. (a) Average specific volume ( $v$ ) versus weight fraction  $w$  of the high molecular weight component. Here, two horizontal dashed lines ( $v_5$  and  $v_{1000}$ ) denote the values for the specific bead volumes of pure solvent ( $N = 5$ ) and pure long chains ( $N = 1000$ ). The red solid dots are the simulation data for the average specific volume  $v$ , and the blue dashed curve is the corresponding ideal result for  $w$ -independent specific volumes of the components,  $v = v_5 + (v_{1000} - v_5)w$ . (b) Mean-square gyration radius  $R_g^2$  of the long chains versus volume fraction  $\phi$ , employing eq 2. (c) Ratio of mean-square end-to-end distance  $R_{ee}^2$  over square gyration radius versus  $\phi$ . (d) Weight-averaged entanglement length  $N_e^*$  calculated by PPA (upper) and Z1 (lower panel) versus  $\phi$ . The red solid dots are the calculated values, and the blue dashed curves are the fitting functions of  $N_e^*(1)\phi^{-\alpha}$  with  $\alpha = 1.25$  and  $1.12$ , respectively, where  $N_e^*(1) = 31.1 \pm 1.1$  (PPA) and  $N_e^*(1) = 43.3 \pm 1.4$  (Z1) are the entanglement lengths of the pure long chain melt ( $\phi = 1$ ) at  $T = 495$  K.

monomers in a straight primitive path segment between two adjacent kinks<sup>55</sup> as the entanglement “length”. All monomers in the same straight segment share the same value of entanglement length, denoted as  $N_e$  for the  $i$ th monomer. We will use weight-averaged values ( $N_e = \sum_{i=1}^N N_e/N$ ) for the whole system in our following discussions. The effect of fixed chain ends to the calculated entanglement length can be corrected, e.g., by<sup>54,56</sup>

$$N_e^* = \frac{N}{N/N_e - 1} \quad (1)$$

where  $N_e^*$  is the normalized entanglement length (length-independent), and we took the approximation of  $N/(N - 1) \approx 1$  when  $N \gg 1$ .

We are going to investigate systems with volume fractions ( $\phi$ ) ranging from  $\phi = 1.0$  (pure melt) to  $\phi = 0.469$ . Details will be given in next section. To study the crystallization behavior, we define the instantaneous stem length  $d$  by the number of successive trans–trans monomers along the long chain at a given time.<sup>50</sup> The trans–trans state is determined by the bending angle  $\theta$  formed by a monomer with its two adjacent monomers, and not by a dihedral angle, due to the peculiar

bending potential as part of the CG-PVA model that exhibits three local minima. A monomer is considered to be in a trans–trans state if its corresponding angle satisfies  $\theta \geq 150^\circ$ . A monomer is considered as crystallized if  $d \geq 15$ .<sup>50</sup> Both the criteria of  $\theta \geq 150^\circ$  and  $d \geq 15$  are obtained from histograms of statistical results at various temperatures from  $T = 0.5$ – $1.0$  and work fairly well compared with other methods. We do not find qualitative differences by varying the threshold over the range of  $d = 13$ – $18$ .<sup>50</sup> Every monomer  $i$  thus carries its value of the corresponding stem length,  $d_i$ . The weight-averaged value,  $d = \sum_i d_i/N$ , will be used in the following discussion. The crystallinity of the whole system, denoted by  $\chi$ , is then obtained directly from the fraction of long chain monomers belonging to crystalline stems, i.e., by the probability that  $d_i$  exceeds 15. We note that this crystallization criterion works well for the quantification of the crystalline state but is unsuitable for the characterization of the early stage of nucleation where  $d$  is increasing to 15.

## ■ GENERATION OF START CONFIGURATIONS

The initial configuration is taken from a pure melt of 100 long chains ( $N = 1000$ ) at  $T = 495$  K after a relaxation of  $3.5 \mu\text{s}$  ( $10^8$  MD steps) at 1 atm. We randomly insert different amounts of

solvent composed of short chains ( $N = 5$ ) into the initial configuration and then relax the systems to obtain equilibrated solutions at the fixed pressure of 1 atm. As the monomer beads of the short chains are identical to those of long chains, the amount of solvent,  $s$ , can be characterized by the number of solvent beads divided by the number of solute beads. The weight fraction of the high molecular weight component is  $w = 1/(1 + s)$ . During the insertion procedure, we steadily increase  $s$  by randomly inserting 200 short chains and then run a short relaxation of 3.5 ps ( $10^5$  MD steps) with a reduced time step of 0.035 fs to remove overlaps of some monomers and to perform a slight enlargement of the simulation box.

Having added short chains to the melt, ten selected initial configurations were chosen ( $s = 0.1, 0.2, \dots, 1.0$  corresponding to weight fractions  $w = 10/11, 5/6, \dots, 1/2$ ) to do relaxation of 2.8  $\mu\text{s}$  ( $8 \times 10^7$  MD steps). We show the properties of three representative systems with  $w = 1$  ( $s = 0$ ),  $2/3$  ( $s = 0.5$ ), and  $1/2$  ( $s = 1.0$ ) during relaxation in Figure 1. In Figure 1a, we display the autocorrelation function of end-to-end vectors ( $X_{ee}(t)$ ) of the long chains, which is defined by  $X_{ee}(t) = \langle \mathbf{R}_{ee}(\tau) \cdot \mathbf{R}_{ee}(\tau + t) \rangle_\tau / \langle \mathbf{R}_{ee}(\tau) \mathbf{R}_{ee}(\tau + t) \rangle_\tau$ , where  $\mathbf{R}_{ee}(t)$  denotes an end-to-end vector at time  $t$ ,  $R_{ee}(t) = |\mathbf{R}_{ee}(t)|$  is its norm, and the symbol  $\langle \rangle_\tau$  stands for average over all chains and all time offsets  $\tau$ . We can see that  $X_{ee}(t)$  decreases to about 0.3 after 2800 ns and that the relaxation is slightly faster for higher diluted solutions.

The short chains act as a good solvent, and the configurations of long chains are swollen during the steady inserting of short chains.<sup>57,58</sup> The mean-square gyration radius ( $\langle R_g^2(t) \rangle$ ) and the ratio of mean-square end-to-end distance over square gyration radius ( $\langle R_{ee}^2(t) \rangle / \langle R_g^2(t) \rangle$ ) of long chains are shown in Figure 1b,c. From Figure 1b, we can see that  $\langle R_g^2(t) \rangle$  stabilizes after about 1400 ns. The ratios of  $\langle R_{ee}^2(t) \rangle / \langle R_g^2(t) \rangle$  are slightly above 6 (of ideal Gaussian chain conformations), as shown in Figure 1c. We note that the gyration radius is smaller than the half of box size to avoid finite size effects.

The relaxation of long chains is very slow and a small change of  $\langle R_g^2(t) \rangle$  does not necessarily signal an equilibrated state. Therefore, we calculated the entanglement lengths to test the equilibration of all the solutions. The weight-averaged entanglement lengths  $N_e^*(t)$  during the relaxation are shown in Figure 1d, by both PPA and Z1 methods. The relaxation of  $N_e^*(t)$  is slower than that of both  $\langle R_g^2(t) \rangle$  and  $\langle R_{ee}^2(t) \rangle / \langle R_g^2(t) \rangle$ . The values of  $N_e^*$  calculated by PPA or Z1 methods can be compared with experimental measurements. From literature we only found an estimated value of  $N_e^* \approx 85$  for aqueous PVA solutions,<sup>59</sup> in rough agreement with our  $N_e^*$  values. For solutions, the  $N_e^*(t)$  seems to stabilize slower. The reason for this might be that the initial states generated by randomly inserting short chains deviate more from their equilibrium ones. From Figure 1d, we can see that the systems are close to their equilibrated states after 2100 ns for all weight fractions studied, as also the  $N_e^*(t)$  values stabilize after that time. It is important to note that these relaxation times represent both certain relaxation of the mixture and the distance of our start configurations from an equilibrium state.

## RESULTS AND DISCUSSION

Results are obtained using the equilibrated start configurations, and averages are sampled during subsequent MD simulations for a duration of 2100–2800 ns at  $T = 495$  K. Long chain conformational properties at different polymer weight fractions are presented in Figure 2. The system volume decreases with

increasing  $w$ , and the average specific monomer volume ( $v$ ) can be extracted from the simulation by the total volume over the total number of monomers (red bullets in Figure 2a). Because of end effects, the specific monomer volumes are  $v_{1000} = 0.06496$  and  $v_5 = 0.07340$  nm<sup>3</sup>, for the pure long and short chains, respectively. Here,  $v_{1000}$  and  $v_5$  are calculated from simulations of long chains (pure melt) and short chains (pure solvent) at  $T = 495$  K and a constant pressure of 1 atm; see the two dashed horizontal lines shown in Figure 2a. The blue dashed line in Figure 2a shows the average specific volume  $v_5 + (v_{1000} - v_5)w$  that corresponds to the ideal situation, where the specific bead volumes  $v_5$  and  $v_{1000}$  of the pure phases are preserved in the mixture. Accordingly, the volume fraction of the long chains ( $\phi$ ) can be expressed in terms of the weight fraction:

$$\phi = \frac{v_{1000}w}{v} \approx \frac{7.7w}{8.7 - w} \quad (2)$$

The investigated volume fractions range from  $\phi = 1.0$  (pure melt) to  $\phi = 0.469$  ( $w = 0.5$ ). In the remainder of this article we will use  $\phi$  instead of  $w$  to characterize the mixture, as most physical quantities are more closely related to  $\phi$ .

Equilibrium values for  $R_g^2$  and  $R_{ee}^2/R_g^2$  versus  $\phi$  are shown in Figure 2b,c, where  $R_g^2$  and  $R_{ee}^2$  are time-averaged mean-square quantities. While the long chains are swollen, their conformations remain nearly Gaussian as the values of  $R_{ee}^2/R_g^2$  almost do not change with  $\phi$ ; they are all only slightly above the 6 of ideal Gaussian chains.

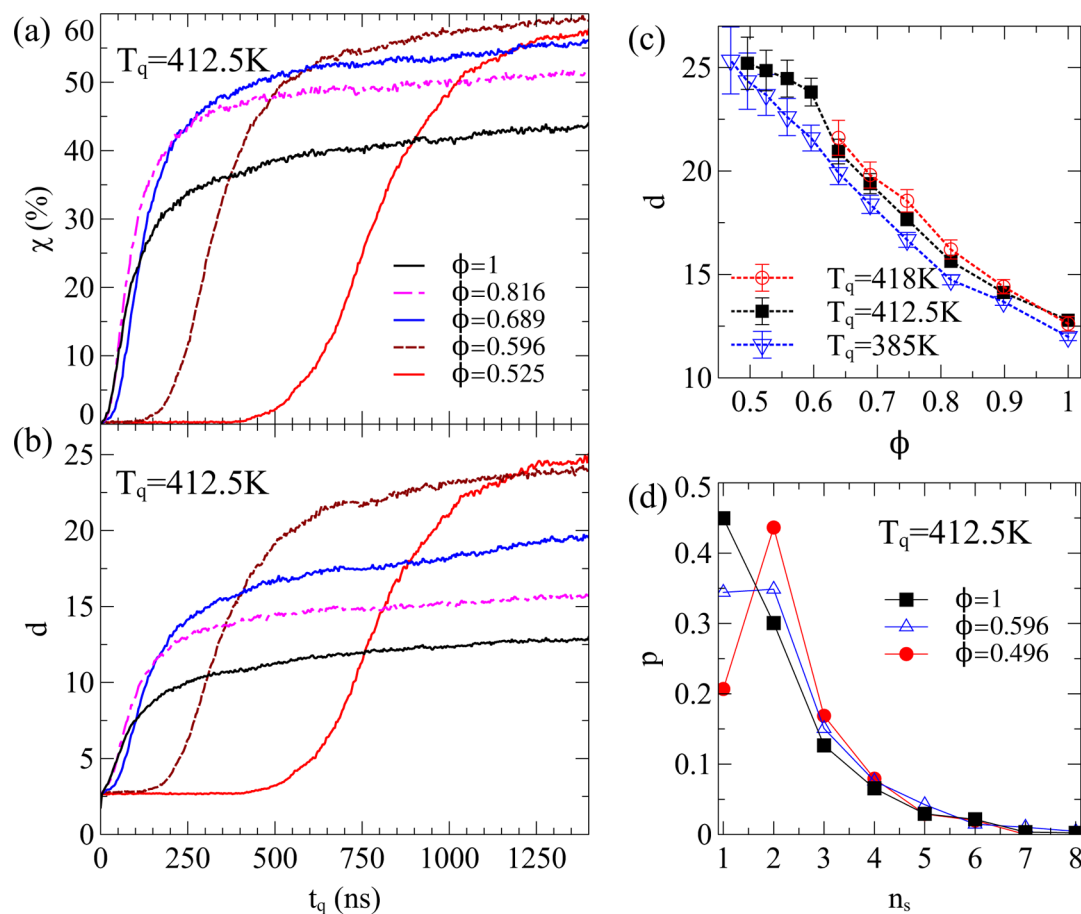
In general, the entanglement length in polymer solutions can be written as<sup>60</sup>

$$N_e^*(\phi) = N_e^*(1)\phi^{-\alpha} \quad (3)$$

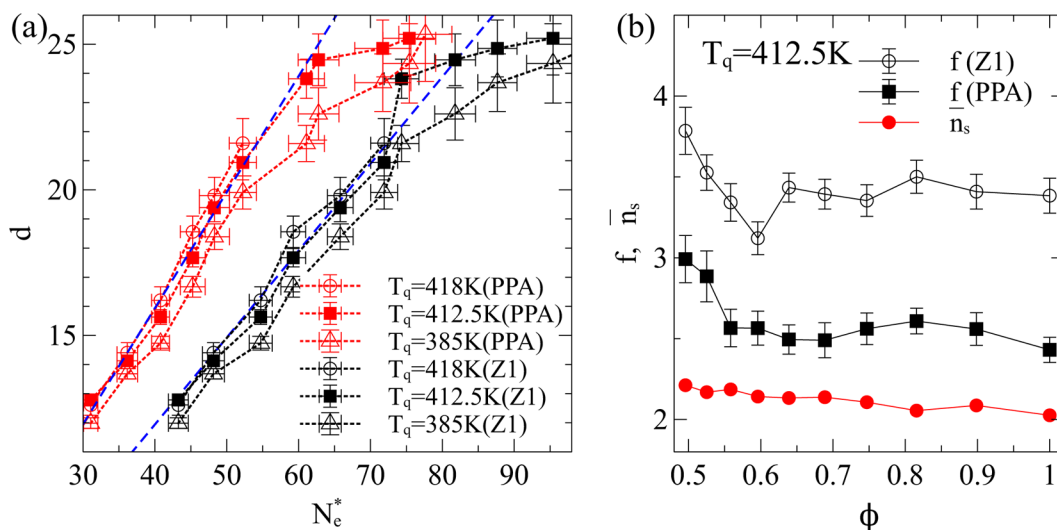
where  $N_e^*(1)$  denotes the entanglement length of the pure melt and the dilution exponent,  $\alpha$ , is a constant. There is no consensus about the exact value of  $\alpha$  in the literature; its value seems to depend on the model of data analysis, the architecture of the polymers, and also the definition of entanglements.<sup>60–62</sup> The blob model of de Gennes suggests a range of  $\alpha$  values, from 1.31 for good solvents to 2.0 for  $\Theta$  solvents. The Colby–Rubinstein conjecture yields  $\alpha = 4/3 = 1.33$  for  $\Theta$  solvents.<sup>60,63</sup> For concentrated solutions, the predicted values vary from 1 to 4/3 and experimental values of  $\alpha$  vary from 1 to 1.7.<sup>60</sup> For example, the PS/OS-2k concentrated solutions indicate  $\alpha \approx 1$ ,<sup>61</sup> while the scaling of PBD/PhO concentrated solutions is captured by  $\alpha \approx 1.29$ .<sup>60</sup>

Figure 2d shows the weight-averaged entanglement lengths at different  $\phi$  via PPA (upper) and Z1 (lower panel). From the fitting curves, we obtain the dilution exponent value as  $\alpha = 1.25$  for PPA and  $\alpha = 1.12$  for Z1; both values are within the scope of 1 and 4/3. Actually, the volume fractions  $\phi$  in our cases are in concentrated regime and the Colby–Rubinstein conjecture should theoretically work and give  $\alpha = 1.33$ ,<sup>60</sup> and thus  $N_e^* \approx 80 \pm 3$  (PPA) and  $N_e^* \approx 101 \pm 3$  (Z1) for the smallest  $\phi$  considered here. Our fitted exponents can thus not rule out this conjecture. Moreover, the chain conformations slightly deviate from ideal Gaussian as shown in Figure 2, which may affect the precise value of  $\alpha$ .

We carried out simulations of isothermal crystallization by instantaneous cooling systems to target quench temperatures, denoted by  $T_q$ . As shown in our previous work, the apparent crystallization temperature of pure CG-PVA long chain melts during continuous cooling is about  $T_c = 429$ – $434$  K, depending on the cooling rate. However, at  $T_q = 429$  K, we did not



**Figure 3.** (a) Crystallinities ( $\chi$ ) for different volume fractions of long chains ( $\phi$ ) during the quench at  $T_q = 412.5$  K. (b) Stem length ( $d$ ) during the quench at  $T_q = 412.5$  K. Here the values are weight-averaged over the whole systems. (c) Weight-averaged stem length ( $d$ ) in the crystalline state formed by supercooling at  $T_q = 418$ , 412.5, and 385 K for different volume fraction ( $\phi$ ). Here, the values are averaged from  $t_q = 1225$  to 1400 ns. We note that at  $T_q = 418$  K the systems with  $\phi < 0.639$  cannot crystallize or reach stabilized crystallinities at the end of 1400 ns, and we only show the results with stabilized crystallines. (d) Normalized probabilities ( $p$ ) for number of crystalline stems in a folded bundle ( $n_s$ ) in the crystalline state formed at  $T_q = 412.5$  K. For a clear view, we only show some selected results of  $\phi$ .



**Figure 4.** (a) Mean stem length  $d$  in the crystalline state formed by supercooling at  $T_q = 418$  K (open circles), 412.5 K (full squares), and 385 K (open triangles) versus entanglement length  $N_c^*$  of the initially homogeneous solutions at  $T = 495$  K, calculated by PPA (red) and Z1 (black) methods. Here both  $d$  and  $N_c^*$  are weight-averaged values. The blue dashed lines are linear interpolants,  $d = N_c^*/f$ , taking into account the higher concentrated regime, with fixed  $f = 2.51$  for PPA and  $f = 3.35$  for Z1. (b) Effective,  $\phi$ -dependent folding factor,  $f = N_c^*/d$  (black), and the average value of number of crystalline stems in a bundle,  $\bar{n}_s$  (red), versus volume fraction  $\phi$  for  $T_q = 412.5$  K.

observe any crystallization for solutions with  $\phi < 0.816$  until 1400 ns. To compare results of different solutions, we used lower quench temperatures with  $T_q = 418, 412.5,$  and  $385$  K. We note that the crystallization in our simulations would be comparable to the regime II of LH theory.

In Figure 3a,b, we show the crystallinity and the weight-averaged stem length during the quench at  $T_q = 412.5$  K. We note that the crystallization degree at  $T_q = 418$  K is similar to  $T_q = 412.5$  K for  $\phi \geq 0.596$ , but we did not observe crystallization at  $T_q = 412.5$  K for  $\phi < 0.596$  after 1400 ns. The induction time of crystallization is increased, and the growth rate is decreased with more solvent (decrease of  $\phi$ ), which can be understood by a less degree of undercooling for systems with smaller relative amounts of long chains. Here we just give a qualitative result and the accurate analysis of growth kinetics requires multiple simulation runs. The mean stem length  $d$  is also decreasing with the increase of  $\phi$  (see Figure 3c). One might explain this by enhanced supercooling and a faster crystallization rate with increasing  $\phi$ . It is important to note that changes of stem lengths at  $T_q = 418, 412.5,$  and  $385$  K for  $\phi > 0.639$  are very small, as shown in Figure 3c. This small difference of stem length cannot be explained by the degree of undercooling. Also, from Figure 3b, we note that the maximum growth rates of stem lengths (maximum slopes of  $d$  vs  $t_q$  curves) under such a supercooling do not differ significantly between different dilutions, while the mean crystalline stem length  $d$  changes substantially. To be more quantitative, the former decreases by factor 1.3, while the latter decreases by factor 2, when comparing  $\phi \approx 0.53$  with  $\phi = 1$ . These results show a decoupling of stem length and growth rate and indicate that the stem length (lamellar thickness) does not result exclusively from a competition between thermal dynamics and growth kinetics, as described by the classic LH theory.

A direct relation between the entanglement length in the amorphous polymer melt at the onset of crystallization and the resulting stem length in the crystalline phase had been revealed earlier.<sup>46,47</sup> Dilution with short, noncrystallizable chains leads to a change of the entanglement length without changing other properties of the system. Thus, it provides an ideal test of the previously found topological principle for thickness selection. In Figure 4a, we show the relation between the crystalline stem length  $d$  and the initial entanglement length  $N_e^*$  before the quenches. We observe a linear relationship between the two quantities for  $\phi > 0.639$ :

$$d = \frac{N_e^*}{f}, \quad f \approx \begin{cases} 2.51, & \text{by PPA} \\ 3.35, & \text{by Z1} \end{cases} \quad (4)$$

The value of  $f$  reflects the average number of tight folds per entanglement length. Interestingly, the folding factor  $f$  can be related with the one recently observed in NMR experiments by Miyoshi et al.,<sup>64–66</sup> describing folded motifs consisting of successively tightly folded stems. The breakdown of the linear relation under more diluted conditions ( $\phi < 0.639$ ) probably has two reasons. The first one is that the crystallization process does not fully complete during the limited simulation time, resulting in underestimated values of  $d$ , particularly for  $\phi < 0.525$ . Another one is that longer untangled segments might allow for larger folding numbers, as indicated by recent NMR experiments.<sup>64–66</sup> The difference between PPA and Z1 is that PPA does dynamic energy minimization of the bead–spring chains to find a configuration residing in an energetic minimum, while Z1 does a geometrical minimization of

infinitely thin chains to find a configuration with shortest disconnected path. We suppose that Z1 might shrink the primitive path more drastically in diluted solutions as the swelling of chain configuration increases the possibility of being tracked into local minima (for the case of PPA).<sup>67</sup>

We note that the  $f$  value is consistent with previous results for pure melts at different initial temperatures,<sup>47</sup> where  $f = 2.48$  for PPA was obtained if we convert the reported value for  $N_e$  to the normalized entanglement length  $N_e^*$ . Therefore, the degree of undercooling may affect the induction time and crystallization rates, but the crystalline stem length seems directly controlled by the initial entanglement lengths. Under supercooling, entanglements are arrested by the high density of nucleation in accord with a growth rate that is faster than the ratio between gyration radius and the disentanglement time. If we consider entanglements like physical cross-links, the situation is similar to crystallization in a rubbery material as discussed by Flory.<sup>68</sup> In our previous studies we have shown that disentanglement makes only a minor contribution under supercooling. This finding remains clearly in contrast with the reeling-in process as assumed by Hoffman and Miller.<sup>6,69</sup>

It is interesting to inspect the changes of chain folds upon varying  $\phi$ . In Figure 3d, we show normalized probabilities  $p(n_s)$  for the number of folding stems per crystallized bundle,  $n_s$ . Here,  $n_s = 1$  means an individual crystalline stem,  $n_s = 2$  stands for a hairpin with two folded crystalline stems, and  $n_s = 3$  represents an arrangement composed of three crystalline stems connected by two hairpin folds. We calculated  $n_s$  by analyzing the crystalline structure via the algorithm described in previous work,<sup>50</sup> which tracks the birth of a crystallized bundle. We can see that under a strong supercooling the crystallization rate is very high, and many individual crystalline stems ( $n_s = 1$ ) are involved in the crystallites. The probability of individual crystalline stems increases with decreasing  $\phi$  due to the decrease of crystallization rate and to the expense of the formation of hairpin folds (see Figure 3d). This result indicates that the chain folds are preferred in slower crystal growth, in agreement with results for the growth of a single crystal from melt by self-seeding.<sup>50</sup> To see if there is a relationship between the folding factor  $f = N_e^*/d$  and the average value of the number of stems in a crystalline bundle,  $\bar{n}_s = \sum p(n_s)n_s$ , both quantities are displayed in Figure 4b. The values of  $f$  and  $\bar{n}_s$  do not differ by more than a factor 2, and both slightly decrease with increasing  $\phi$ . The values of  $\bar{n}_s$  in the range of 2.0–2.2 are almost identical with those reported for pure melts quenched from different initial temperatures.<sup>47</sup> We note that the values of  $\bar{n}_s$  and their trend to exhibit a slow decrease with increasing  $\phi$  are consistent with recent experimental NMR results:  $\bar{n}_s \geq 1.7$ – $2$  for melts and  $\bar{n}_s \geq 8$  for dilute solutions.<sup>64–66</sup> The behavior of the folding factor  $f(\phi)$  in concentrated conditions ( $\phi > 0.639$ ) is in overall agreement with  $\bar{n}_s(\phi)$ . The larger qualitative deviation between  $f$  and  $\bar{n}_s$  at more diluted conditions ( $\phi < 0.639$ ) is eventually caused by the underestimation of  $d$  at the limited quench time, while  $\bar{n}_s$  is of course unaffected by the quench time.

As reported in our previous works, entanglements are almost preserved during the crystallization in melts. This observation leads us to propose that the initial state of entanglement directly controls the crystalline stem length (lamellar thickness). For this conclusion it was important to recognize that the entanglement length is reduced by stiffening of the chains in the undercooled melt and that the temperature dependence of the entanglement length follows the same empirical law with

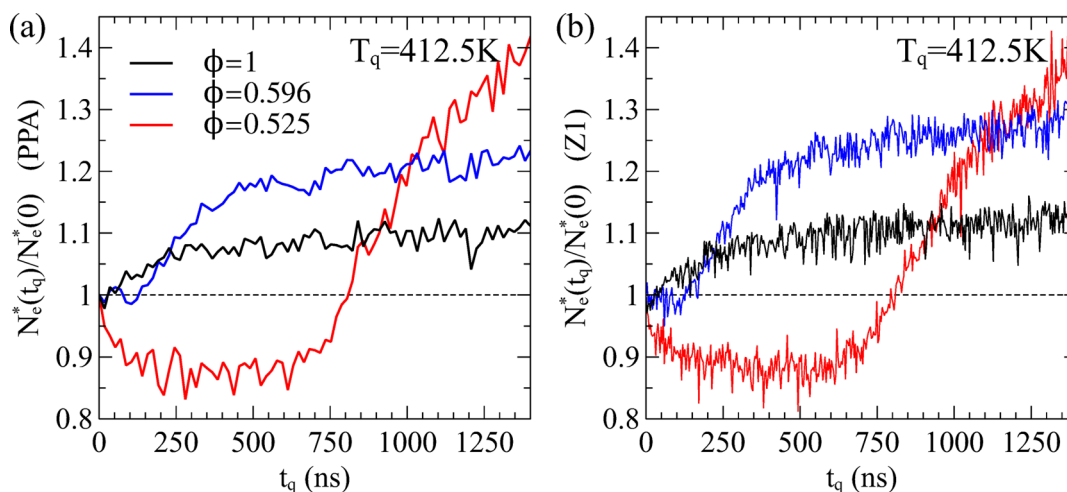


**Figure 5.** Entanglement length changes during the crystallization at  $T_q = 412.5$  K, calculated by PPA (a) and Z1 (b). Here, the ratios of  $N_e^*(t_q)$  over  $N_e^*(t_q = 0)$  are displayed to reflect the degree of disentanglement during crystallization.

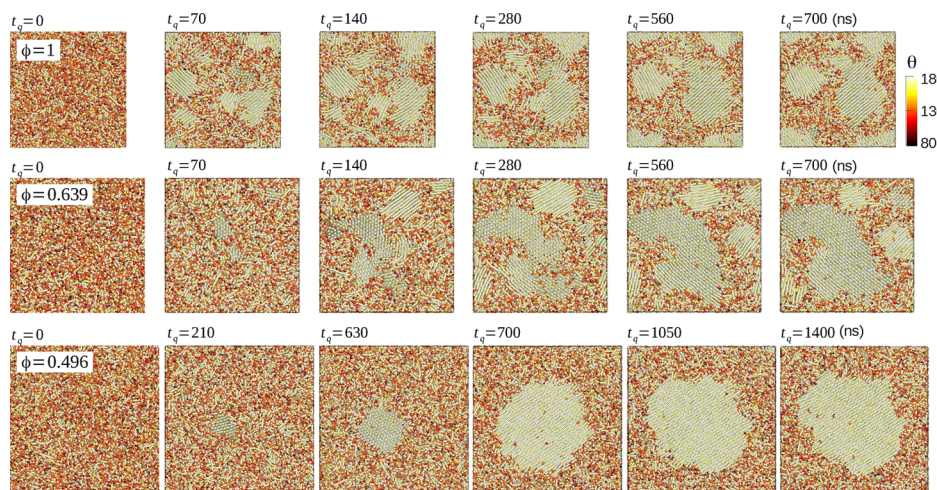


**Figure 6.** Section views of snapshots taken during crystallization at  $T_q = 412.5$  K for three different volume fractions: (top) pure melt,  $\phi = 1$ , (center) highly concentrated solution,  $\phi = 0.639$ , and (bottom) concentrated solution,  $\phi = 0.496$ . Here, monomers are colored by their bending angle ( $\theta$ ) that is used to recognize trans–trans conformations and crystalline regions, to calculate the mean stem length and the degree of crystallization. The color bar is shown at the right top corner. The system size increases with decreasing  $\phi$  as we add solvent particles during preparation of the equilibrium samples at  $T = 495$  K. These configurations are shown at  $t_q = 0$ , and the quench temperature  $T_q$  is kept constant at  $t_q > 0$ .

temperature as the stem length.<sup>47</sup> It is therefore interesting to follow the evolution of the entanglement length also for concentrated solutions. In Figure 5, we display the ratios of  $N_e^*(t_q)$  over  $N_e^*(t_q = 0)$  at  $T_q = 412.5$  K. For the pure melt ( $\phi = 1$ ), the ratio approaches a value of 1.1, indicating a slight disentanglement. The initial entanglements are thus almost preserved. We observe that a part of the disentanglement is caused by the reorganization after homogeneous crystallization ( $t_q > 350$  ns), as the coarse-grained monomer beads can still slowly slide in the crystalline state.<sup>50</sup> The degree of disentanglement is a little larger in less concentrated solutions. For example, the ratio of  $N_e^*(t_q)/N_e^*(0)$  is about 1.4 for  $\phi = 0.525$  at the end of the simulation. The decrease of  $N_e^*(t_q)$  before crystallization is due to the temperature drop, as discussed in our previous work for melts,<sup>47</sup> and thus a key to understand the temperature dependent thickness selection in concentrated polymer solutions as well.

Snapshots taken during crystallization at  $T_q = 412.5$  K for  $\phi = 1$ ,  $\phi = 0.639$ , and  $\phi = 0.496$  are shown for comparison in Figure 6. One can see that the growth rate decreases with

decreasing  $\phi$ , resulting in higher crystallinity, as already quantified in Figure 3a. One can also see that the crystallization within the pure melt proceeds from a larger amount of nucleation sites and is thus apparently more homogeneous. With the decrease of  $\phi$ , the growth rate is reduced. The slower growth rate allows more relaxation time for the formation of chain folds and results in larger  $\bar{n}_c$ , as shown in Figure 4d. From Figure 6, we can see that for  $\phi = 0.496$  there is only one crystallite in the viewing section and there are only two crystallites in the whole simulated system (another one is invisible from the section view). A qualitatively analogous behavior was found in the so-called elastic Lennard-Jones (LJ) system,<sup>70–72</sup> a permanently spring-connected network of LJ particles. At sufficiently low spring coefficient and temperature, crystalline LJ clusters tend to form due to short-ranged LJ attraction, but the formation of both a single or an infinite cluster is prevented by the spring-mediated connectivity between clusters, which effectively serves as a long-range repulsion due to periodic boundary conditions. In the present condensed polymer solutions, the crystalline regions are

interconnected by long chains. Such bridging chains could stabilize the network of crystalline regions, providing a direct analogy to the elastic LJ model.

## CONCLUSIONS

In conclusion, we presented MD simulation results for concentrated solutions of long chains where the solvent is composed of short chains of the same species. We followed the dynamics and statistical properties of the crystallization process of the high molecular weight component at different concentrations. In particular, we have studied the entanglement properties of these systems using two variants (PPA and Z1) to calculate the primitive path and the entanglement length. The equilibrium weight-averaged entanglement length in the concentrated solution above the point of crystallization ( $T_c$ ) is found to scale with a power of volume fraction. Upon crystallization, we show that there is a decoupling of stem length and growth rate. A central result of our work is that the weight-averaged stem length (lamellar thickness) is proportional to the initial entanglement length in the homogeneous solution, where the factor of proportionality,  $f$ , defines the number of stems in tight folds formed in one entangled sequence. The average value of  $f$  is found almost unchanged compared to pure melts at different initial temperatures,<sup>47</sup> while it is moderately decreasing with increasing volume fraction of the long chain component. Both the values of folding numbers and the trend with respect to concentration are in agreement with recent experimental results.<sup>64–66</sup> Despite the different crystallization rates and the amount and size of crystalline regions, our previously proposed hypothesis that the entanglement length directly controls the lamellar thickness can explain our current results in concentrated solutions.<sup>46,47</sup> The idea behind is to treat entanglements like physical cross-links similar to crystallization in a rubbery material, as discussed by Flory,<sup>68</sup> rather than to assume disentanglement via reptation as proposed by the LH theory.<sup>69</sup> Our present results for concentrated polymer solutions may help to shed light on the open issue of a full understanding of polymer crystallization.

## AUTHOR INFORMATION

### Corresponding Author

\*E-mail: luochuanfu@gmail.com (C.L.).

### ORCID

Chuanfu Luo: 0000-0002-4911-7870

### Notes

The authors declare no competing financial interest.

## ACKNOWLEDGMENTS

C.L. and J.U.S. gratefully acknowledge the financial support by German Research Foundation of DFG (SO 277/6-2) and computing time from ZIH of TU-Dresden. M.K. acknowledges financial support by the Swiss National Foundation through grant SNF 200021-156106.

## REFERENCES

- (1) Wunderlich, B., Ed.; *Macromolecular Physics: 2. Crystal Nucleation, Growth, Annealing*; Academic Press: New York, 1978.
- (2) Strobl, G. *The Physics of Polymers*, 3rd ed.; Springer: Berlin, 2007.
- (3) Cheng, S. Z. D., Ed.; *Phase Transitions in Polymers: The Role of Metastable States*; Elsevier B.V.: Oxford, 2008.
- (4) Sommer, J.-U.; Reiter, G., Eds.; *Polymer Crystallization: Observations, Concepts and Interpretations*; Lecture Notes in Physics; Springer: Berlin, 2003; Vol. 606.

- (5) Reiter, G.; Strobl, G., Eds.; *Progress in Understanding of Polymer Crystallization*; Lecture Notes in Physics; Springer: Berlin, 2007; Vol. 714.
- (6) Hoffman, J. D. Thermodynamic driving force in nucleation and growth processes. *J. Chem. Phys.* **1958**, *29*, 1192–1193.
- (7) Lauritzen, J. I.; Hoffman, J. D. Extension of the theory of growth of chain-folded polymer crystals to large undercoolings. *J. Appl. Phys.* **1973**, *44*, 4340–4352.
- (8) Hoffman, J. D.; Davis, G. T.; Lauritzen, J., John, I. In *Treatise on Solid State Chemistry*; Hannay, N., Ed.; Springer: New York, 1976; pp 497–614.
- (9) Strobl, G. Colloquium: Laws controlling crystallization and melting in bulk polymers. *Rev. Mod. Phys.* **2009**, *81*, 1287.
- (10) Sadler, D. M.; Gilmer, G. H. Rate-theory model of polymer crystallization. *Phys. Rev. Lett.* **1986**, *56*, 2708.
- (11) Sadler, D. M. New explanation for chain folding in polymers. *Nature* **1987**, *326*, 174–177.
- (12) Olmsted, P. D.; Poon, W. C. K.; McLeish, T. C. B.; Terrill, N. J.; Ryan, A. J. Spinodal-assisted crystallization in polymer melts. *Phys. Rev. Lett.* **1998**, *81*, 373–376.
- (13) Strobl, G. Crystallization and melting of bulk polymers: New observations, conclusions and a thermodynamic scheme. *Prog. Polym. Sci.* **2006**, *31*, 398–442.
- (14) Chen, C.-M.; Higgs, P. Monte-Carlo simulations of polymer crystallization in dilute solution. *J. Chem. Phys.* **1998**, *108*, 4305.
- (15) Doye, J. P. K.; Frenkel, D. Crystallization of a polymer on a surface. *J. Chem. Phys.* **1998**, *109*, 10033.
- (16) Fujiwara, S.; Sato, T. Molecular dynamics simulation of structure formation of short chain molecules. *J. Chem. Phys.* **1999**, *110*, 9757.
- (17) Fujiwara, S.; Sato, T. Molecular dynamics simulation of structural formation of short polymer chains. *Phys. Rev. Lett.* **1998**, *80*, 991.
- (18) Gee, R. H.; Lacevic, N. M.; Fried, L. E. Atomistic simulations of spinodal phase separation preceding polymer crystallization. *Nat. Mater.* **2006**, *5*, 39–43.
- (19) Hu, W. Chain folding in polymer melt crystallization studied by dynamic Monte Carlo simulations. *J. Chem. Phys.* **2001**, *115*, 4395.
- (20) Hu, W.; Frenkel, D.; Mathot, V. B. F. Intramolecular nucleation model for polymer crystallization. *Macromolecules* **2003**, *36*, 8178–8183.
- (21) Hu, W.; Cai, T.; Ma, Y.; Hobbs, J. K.; Farrance, O.; Reiter, G. Polymer crystallization under nano-confinement of droplets studied by molecular simulations. *Faraday Discuss.* **2009**, *143*, 129.
- (22) Koyama, A.; Yamamoto, T.; Fukao, K.; Miyamoto, Y. Molecular dynamics simulation of polymer crystallization from an oriented amorphous state. *Phys. Rev. E* **2002**, *65*, 050801.
- (23) Meyer, H.; Müller-Plathe, F. Formation of chain-folded structures in supercooled polymer melts. *J. Chem. Phys.* **2001**, *115*, 7807–7810.
- (24) Meyer, H.; Müller-Plathe, F. Formation of chain-folded structures in supercooled polymer melts examined by MD simulations. *Macromolecules* **2002**, *35*, 1241–1252.
- (25) Muthukumar, M. Modeling polymer crystallization. *Adv. Polym. Sci.* **2005**, *191*, 241–274.
- (26) Sommer, J.-U.; Reiter, G. Polymer crystallization in quasi-2 dimensions: Part II: Kinetic models. *J. Chem. Phys.* **2000**, *112*, 4384–4393.
- (27) Vettorel, T.; Meyer, H. Coarse graining of short polyethylene chains for studying polymer crystallization. *J. Chem. Theory Comput.* **2006**, *2*, 616–629.
- (28) Welch, P.; Muthukumar, M. Molecular mechanisms of polymer crystallization from solution. *Phys. Rev. Lett.* **2001**, *87*, 218302.
- (29) Yamamoto, T.; Orimi, N.; Urakami, N.; Sawada, K. Molecular dynamics modeling of polymer crystallization: from simple polymers to helical ones. *Faraday Discuss.* **2005**, *128*, 75.
- (30) Yamamoto, T. Molecular dynamics simulations of steady-state crystal growth and homogeneous nucleation in polyethylene-like polymer. *J. Chem. Phys.* **2008**, *129*, 184903.

- (31) Yamamoto, T.; Nozaki, K.; Yamaguchi, A.; Urakami, N. Molecular simulation of crystallization in n-alkane ultrathin films: Effects of film thickness and substrate attraction. *J. Chem. Phys.* **2007**, *127*, 154704.
- (32) Yu, X.; Kong, B.; Yang, X. Molecular dynamics study on the crystallization of a cluster of polymer chains depending on the initial entanglement structure. *Macromolecules* **2008**, *41*, 6733–6740.
- (33) Ni, R.; Dijkstra, M. Effect of bond length fluctuations on crystal nucleation of hard bead chains. *Soft Matter* **2012**, *9*, 365–369.
- (34) Zerze, H.; Mittal, J.; McHugh, A. J. Ab initio crystallization of alkanes: Structure and kinetics of nuclei formation. *Macromolecules* **2013**, *46*, 9151–9157.
- (35) Yi, P.; Locker, C. R.; Rutledge, G. C. Molecular dynamics simulation of homogeneous crystal nucleation in polyethylene. *Macromolecules* **2013**, *46*, 4723–4733.
- (36) Karayiannis, N. C.; Foteinopoulou, K.; Laso, M. The characteristic crystallographic element norm: A descriptor of local structure in atomistic and particulate systems. *J. Chem. Phys.* **2009**, *130*, 074704.
- (37) Karayiannis, N. C.; Foteinopoulou, K.; Abrams, C. F.; Laso, M. Modeling of crystal nucleation and growth in athermal polymers: self-assembly of layered nano-morphologies. *Soft Matter* **2010**, *6*, 2160–2173.
- (38) Karayiannis, N. C.; Foteinopoulou, K.; Laso, M. Entropy-driven crystallization in dense systems of athermal chain molecules. *Phys. Rev. Lett.* **2009**, *103*, 045703.
- (39) Dijkstra, M.; van Roij, R.; Roth, R.; Fortini, A. Effect of many-body interactions on the bulk and interfacial phase behavior of a model colloid-polymer mixture. *Phys. Rev. E* **2006**, *73*, 041404.
- (40) Hikosaka, M.; Amano, K.; Rastogi, S.; Keller, A. Lamellar thickening growth of an extended chain single crystal of polyethylene. I. Pointers to a new crystallization mechanism of polymers. *Macromolecules* **1997**, *30*, 2067–2074.
- (41) Hikosaka, M.; Watanabe, K.; Okada, K.; Yamazaki, S. Topological mechanism of polymer nucleation and growth - the role of chain sliding diffusion and entanglement. *Adv. Polym. Sci.* **2005**, *191*, 137–186.
- (42) Lippits, D. R.; Rastogi, S.; Talebi, S.; Bailly, C. Formation of entanglements in initially disentangled polymer melts. *Macromolecules* **2006**, *39*, 8882–8885.
- (43) Lippits, D. R.; Rastogi, S.; Höhne, G. W. H.; Mezari, B.; Magusin, P. C. M. M. Heterogeneous distribution of entanglements in the polymer melt and its influence on crystallization. *Macromolecules* **2007**, *40*, 1004–1010.
- (44) Rastogi, S.; Lippits, D. R.; Peters, G. W. M.; Graf, R.; Yao, Y.; Spiess, H. W. Heterogeneity in polymer melts from melting of polymer crystals. *Nat. Mater.* **2005**, *4*, 635–641.
- (45) Luo, C.; Sommer, J.-U. Disentanglement of linear polymer chains toward unentangled crystals. *ACS Macro Lett.* **2013**, *2*, 31–34.
- (46) Luo, C.; Sommer, J.-U. Frozen topology: Entanglements control nucleation and crystallization in polymers. *Phys. Rev. Lett.* **2014**, *112*, 195702.
- (47) Luo, C.; Sommer, J.-U. Role of thermal history and entanglement related thickness selection in polymer crystallization. *ACS Macro Lett.* **2016**, *5*, 30–34.
- (48) Luo, C.; Sommer, J.-U. Coding coarse grained polymer model for LAMMPS and its application to polymer crystallization. *Comput. Phys. Commun.* **2009**, *180*, 1382–1391.
- (49) Luo, C.; Sommer, J.-U. Coexistence of melting and growth during heating of a semicrystalline polymer. *Phys. Rev. Lett.* **2009**, *102*, 147801.
- (50) Luo, C.; Sommer, J.-U. Growth pathway and precursor states in single lamellar crystallization. *Macromolecules* **2011**, *44*, 1523–1529.
- (51) Fritz, D.; Koschke, K.; Harmandaris, V. A.; van der Vegt, N. F.; Kremer, K. Multiscale modeling of soft matter: scaling of dynamics. *Phys. Chem. Chem. Phys.* **2011**, *13*, 10412–10420.
- (52) Plimpton, S. Fast parallel algorithms for short-range molecular dynamics. *J. Chem. Phys.* **1995**, *101*, 1–9.
- (53) Everaers, R.; Sukumaran, S. K.; Grest, G. S.; Svaneborg, C.; Sivasubramanian, A.; Kremer, K. Rheology and microscopic topology of entangled polymeric liquids. *Science* **2004**, *303*, 823–826.
- (54) Kröger, M. Shortest multiple disconnected path for the analysis of entanglements in two- and three-dimensional polymeric systems. *Comput. Phys. Commun.* **2005**, *168*, 209–232.
- (55) Foteinopoulou, K.; Karayiannis, N. C.; Mavrantzas, V. G.; Kröger, M. Primitive path identification and entanglement statistics in polymer melts: Results from direct topological analysis on atomistic polyethylene models. *Macromolecules* **2006**, *39*, 4207–4216.
- (56) Hoy, R. S.; Foteinopoulou, K.; Kröger, M. Topological analysis of polymeric melts: Chain-length effects and fast-converging estimators for entanglement length. *Phys. Rev. E* **2009**, *80*, 031803.
- (57) de Gennes, P.-G. *Scaling Concepts in Polymer Physics*; Cornell University Press: Ithaca, NY, 1979.
- (58) Lang, M.; Rubinstein, M.; Sommer, J.-U. Conformations of a long polymer in a melt of shorter chains: Generalizations of the Flory theorem. *ACS Macro Lett.* **2015**, *4*, 177–181.
- (59) Tao, J.; Shivkumar, S. Molecular weight dependent structural regimes during the electrospinning of PVA. *Mater. Lett.* **2007**, *61*, 2325–2328.
- (60) Heo, Y.; Larson, R. G. Universal scaling of linear and nonlinear rheological properties of semidilute and concentrated polymer solutions. *Macromolecules* **2008**, *41*, 8903–8915.
- (61) Huang, Q.; Mednova, O.; Rasmussen, H. K.; Alvarez, N. J.; Skov, A. L.; Almdal, K.; Hassager, O. Concentrated polymer solutions are different from melts: Role of entanglement molecular weight. *Macromolecules* **2013**, *46*, 5026–5035.
- (62) van Ruymbek, E.; Masubuchi, Y.; Watanabe, H. Effective value of the dynamic dilution exponent in bidisperse linear polymers: From 1 to 4/3. *Macromolecules* **2012**, *45*, 2085–2098.
- (63) Larson, R. G. Combinatorial rheology of branched polymer melts. *Macromolecules* **2001**, *34*, 4556–4571.
- (64) Hong, Y.-I.; Koga, T.; Miyoshi, T. Chain trajectory and crystallization mechanism of a semicrystalline polymer in melt- and solution-grown crystals as studied using <sup>13</sup>C-<sup>13</sup>C double-quantum NMR. *Macromolecules* **2015**, *48*, 3282–3293.
- (65) Yuan, S.; Li, Z.; Hong, Y.-I.; Ke, Y.; Kang, J.; Kamimura, A.; Otsubo, A.; Miyoshi, T. Folding of polymer chains in the early stage of crystallization. *ACS Macro Lett.* **2015**, *4*, 1382–1385.
- (66) Li, Z.; Hong, Y.-I.; Yuan, S.; Kang, J.; Kamimura, A.; Otsubo, A.; Miyoshi, T. Determination of chain-folding structure of isotactic polypropylene in melt-grown crystals by <sup>13</sup>C-<sup>13</sup>C double quantum NMR and selective isotopic labeling. *Macromolecules* **2015**, *48*, 5752–5760.
- (67) Shanbhag, S.; Kröger, M. Primitive path networks generated by annealing and geometrical methods: Insights into differences. *Macromolecules* **2007**, *40*, 2897–2903.
- (68) Flory, P. J. Thermodynamics of crystallization in high polymers. I. Crystallization induced by stretching. *J. Chem. Phys.* **1947**, *15*, 397–408.
- (69) Hoffman, J. D.; Miller, R. L. Kinetics of crystallization from the melt and chain folding in polyethylene fractions revisited: theory and experiment. *Polymer* **1997**, *38*, 3151–3212.
- (70) Peleg, O.; Kröger, M.; Hecht, I.; Rabin, Y. Filamentous networks in phase-separating two-dimensional gels. *Europhys. Lett.* **2007**, *77*, 58007.
- (71) Fransson, S.; Peleg, O.; Loren, N.; Hermansson, A.-M.; Kröger, M. Modelling and confocal microscopy of biopolymer mixtures in confined geometries. *Soft Matter* **2010**, *6*, 2713–2722.
- (72) Peleg, O.; Kröger, M.; Rabin, Y. Model of microphase separation in two-dimensional gels. *Macromolecules* **2008**, *41*, 3267–3275.